Supplemental Information

Supplemental Figures

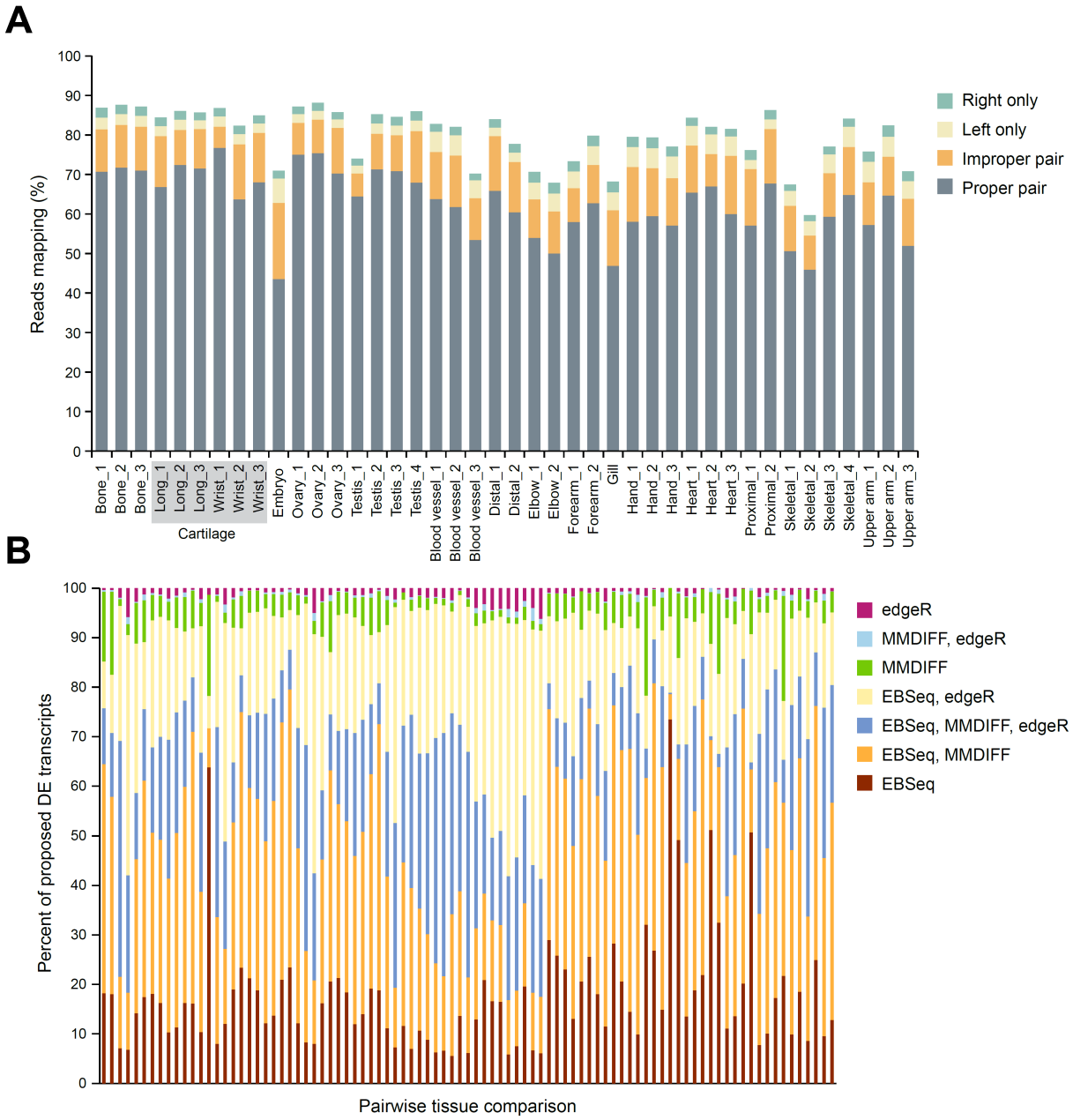

Figure S1. Transcriptome read representation and comparison of methods for differential gene expression analysis. Related to Figure 1 and Table 1. (A) Approximately 80% of RNA-Seq reads from each sample and replicate are represented by the transcriptome assembly. (B) Most transcripts identified as significantly differentially expressed were agreed upon by at least two different computational methods.

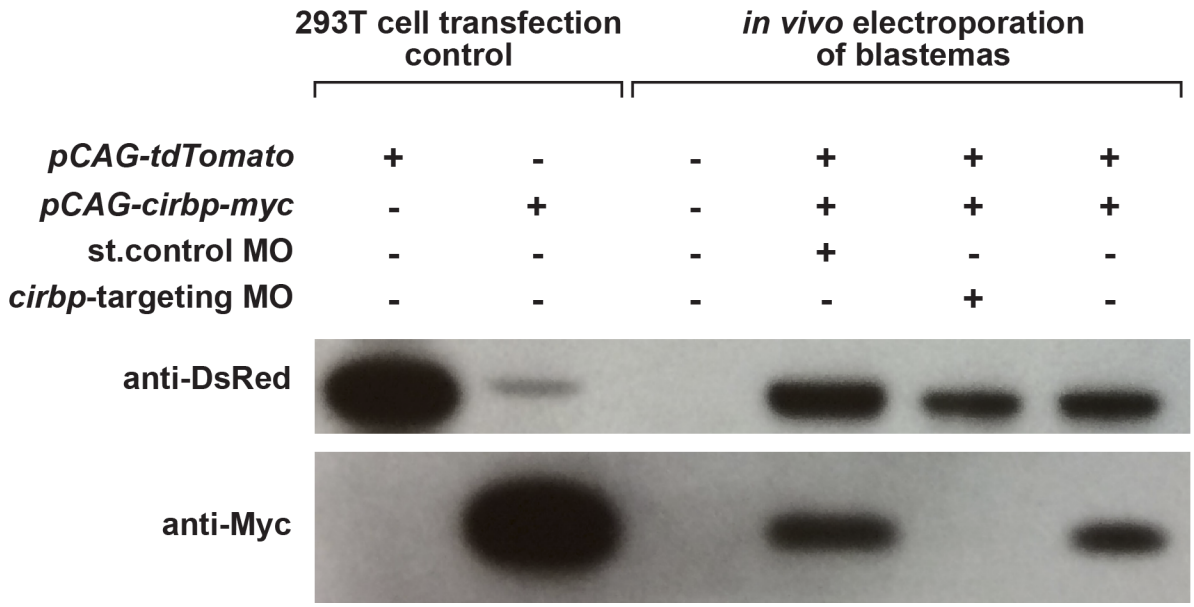

Figure S2. Administration of *cirbp*-targeting morpholino diminishes CIRBP protein level in axolotl tissue. Related to Figure 4. Shown is a western blot labeled with anti-DsRed (top) and anti-myc (bottom) antibodies. On the left are protein samples from HEK293T cells transfected with DNA constructs as shown for validation of protein size and as positive controls. On the right are protein samples from blastemas electroporated with DNA constructs and either the standard control morpholino (st. control MO) or the *cirbp*-targeting morpholino (*cirbp*-targeting MO). Each lane was loaded with 2 μg of total protein.

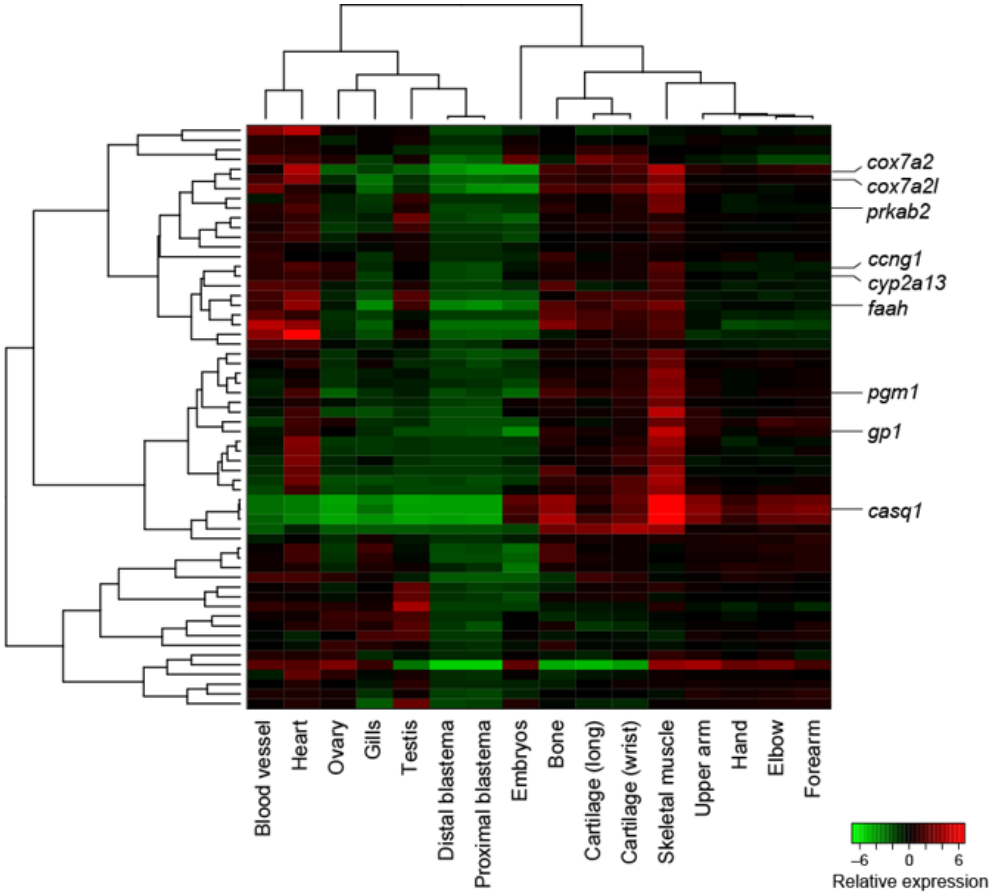

Figure S3. Transcripts found globally repressed in blastemal tissue. Related to Figure 3. Many of the transcripts repressed in blastemal tissue are found highly expressed in skeletal muscle tissue.

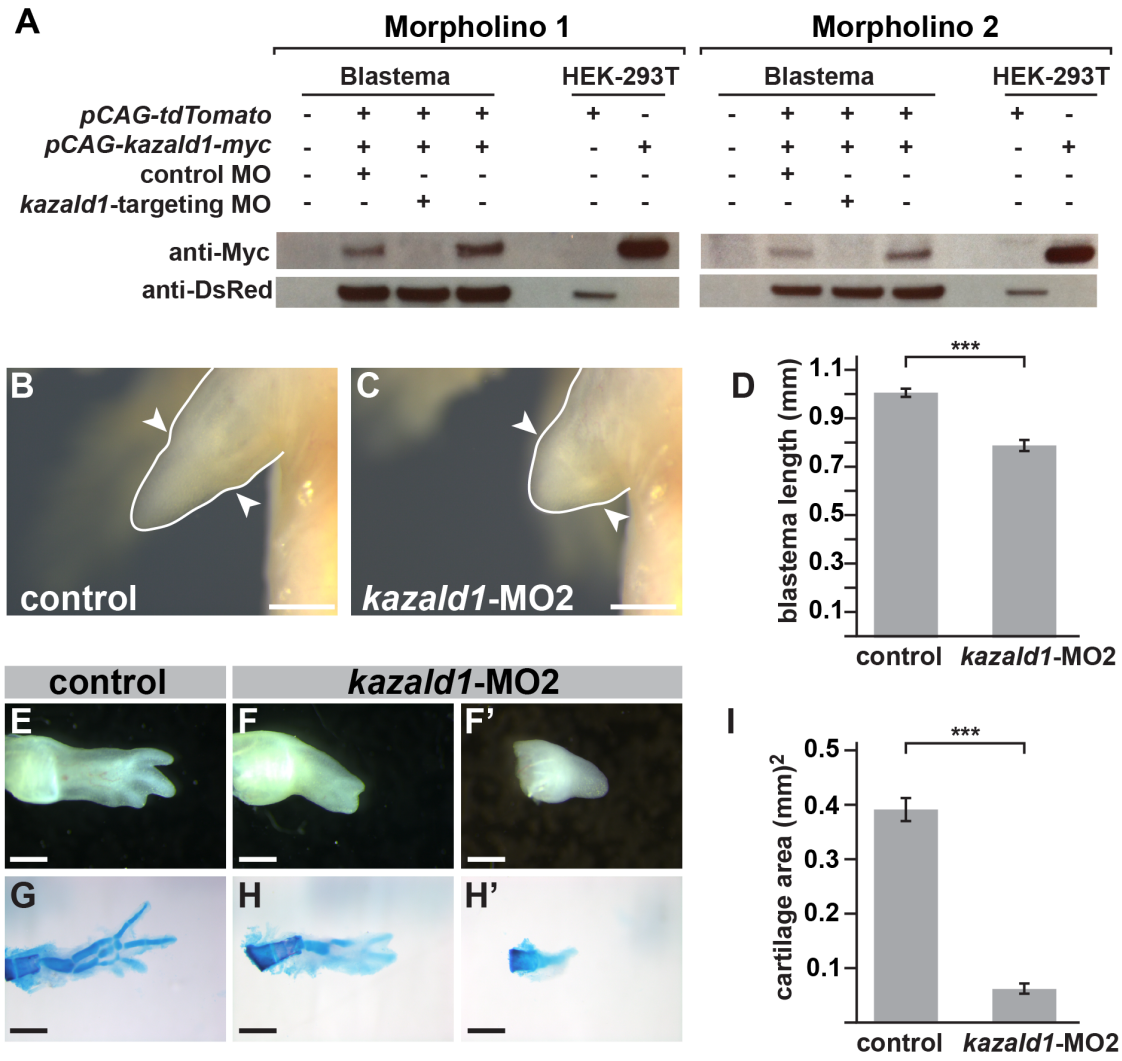

Figure S4. Administration of *kazald1*-targeting morpholinos diminish Kazd1 protein level in blastema cells and a second *kazald1*-targeting morpholino also disrupts regeneration. Related to Figure 5. (A) Shown are western blots probed with anti-myc (top) and anti-DsRed (bottom). Left blot is control morpholino (MO) and *kazald1*-targeting MO for targeting sequence 1, right blot is control MO2 and *kazald1*-targeting MO2; left four lanes are protein samples from limb blastemas electroporated with DNA constructs shown and with the *kazald1*-targeting MO or the related control MO (inverted sequence). Empty lane separates blastema samples from 293T cell samples. 293T cell protein samples transfected with individual DNA constructs were used as the positive controls and to verify size. (B-D) MO2 administration impairs blastema growth. (B-C) Regenerating limbs at 19 days post-amputation treated with control (B, inverted MO2 sequence) or a second *kazald1*-targeting morpholino (*kazald1*-MO2) (C); quantified in (D). (D-H) MO2 administration causes a delay in chondrification. (D-G') Whole-mount brightfield images (top row, E-F') of regenerating limbs with Alcian blue-stained skeleton pictured below (G-H'). Limbs were harvested at 28 days post-amputation. (I) Quantification of cartilage area in control versus *kazald1*-MO2-treated. Control refers to inverted MO sequence. Scale bar is 1 mm. *** indicates $p<0.001$ and error bars are SEM. Arrowheads mark amputation plane in each image.

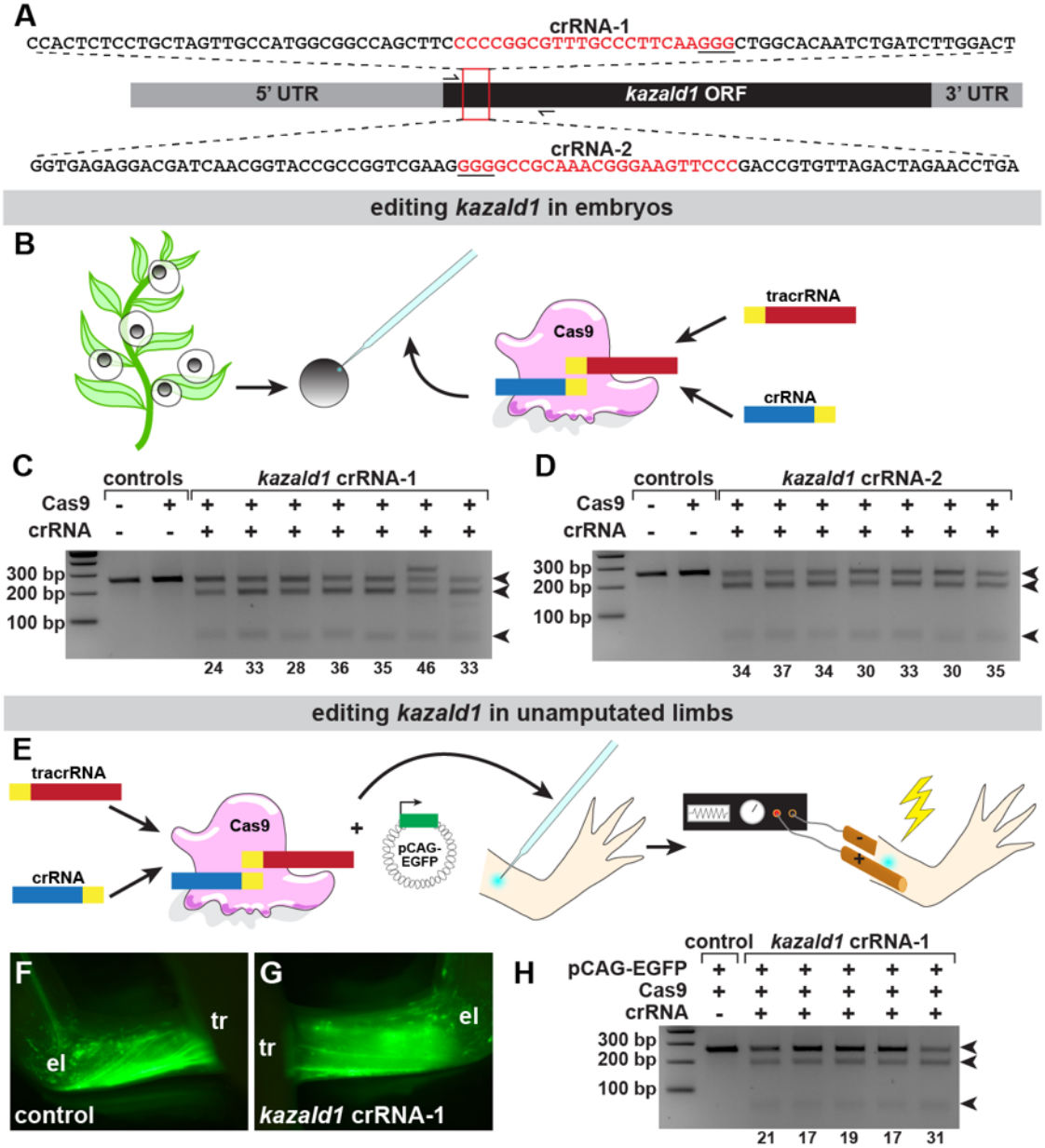

Figure S5. CRISPR-mediated deletions in *kazald1* locus in embryos and unamputated limbs. Related to Figure 5. (A) *Kazald1* genomic locus and targeting scheme. Primers for PCR amplification for genotyping are indicated. (B) Experimental schematic for targeting in embryos via injection. (C-D) Embryo genotyping via PCR followed by T7 endonuclease assay for embryos injected with crRNA-1 (C) and crRNA-2 (D). (E) Experimental schematic for targeting in unamputated limbs via electroporation. (F-G) EGFP expression in control (F, left limb) and crRNA-1-treated (G, right limb) limbs at 25 days post-electroporation. Landmarks: el (elbow), tr (trunk). (H) Limb genotyping via PCR followed by T7 endonuclease assay. For all genotyping, each lane indicates an individual specimen. Editing efficiency is estimated by the indel percentage beneath each lane.

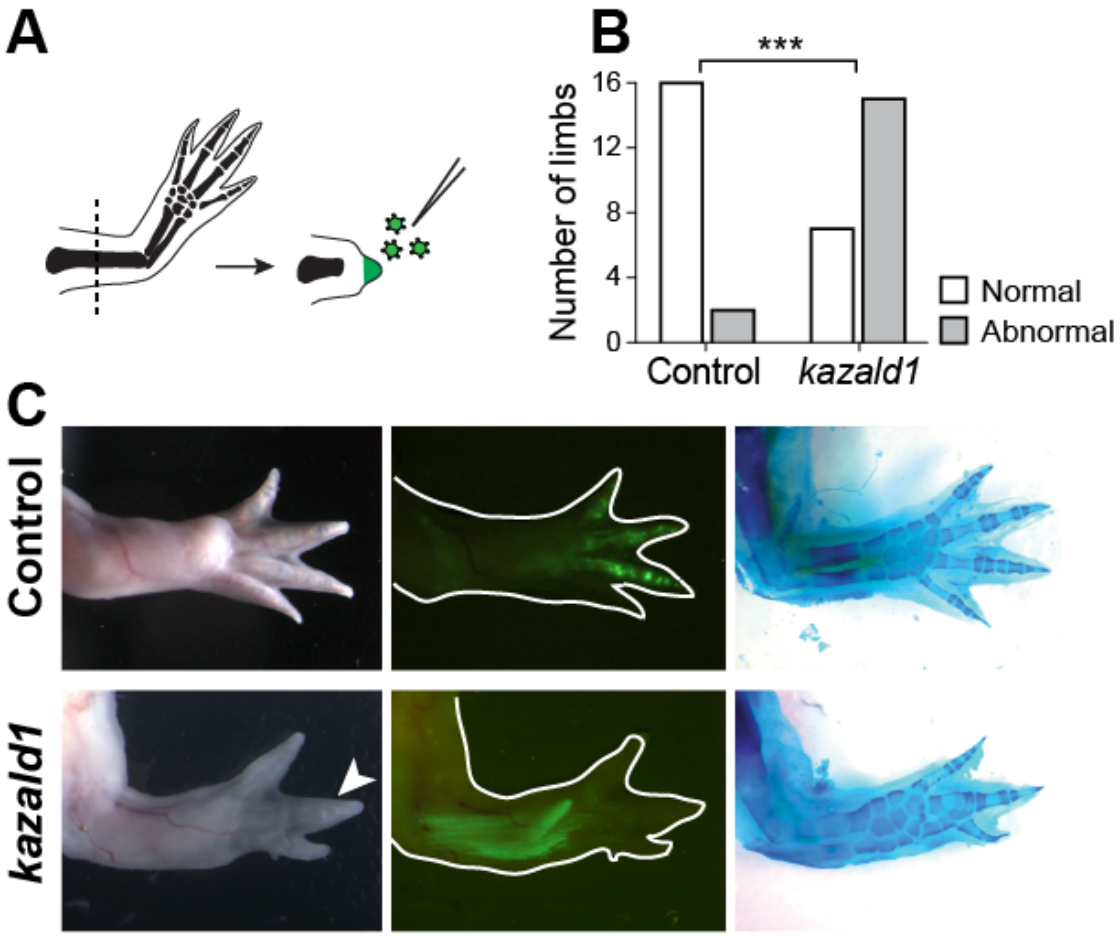

Figure S6. Expression of the most robust blastema marker must be temporally or spatially restricted to achieve perfect regeneration. Related to Figure 5. (A) Experimental setup for virus-driven constitutive misexpression. (B) Prolonged misexpression of *kazald1* causes profound regenerative defects as compared to controls (n=22 experimental, 18 control; p=0.004 with Fisher's exact test). (C) The most common defect observed was syndactyly (indicated by arrow). Scale bar is 500 microns.

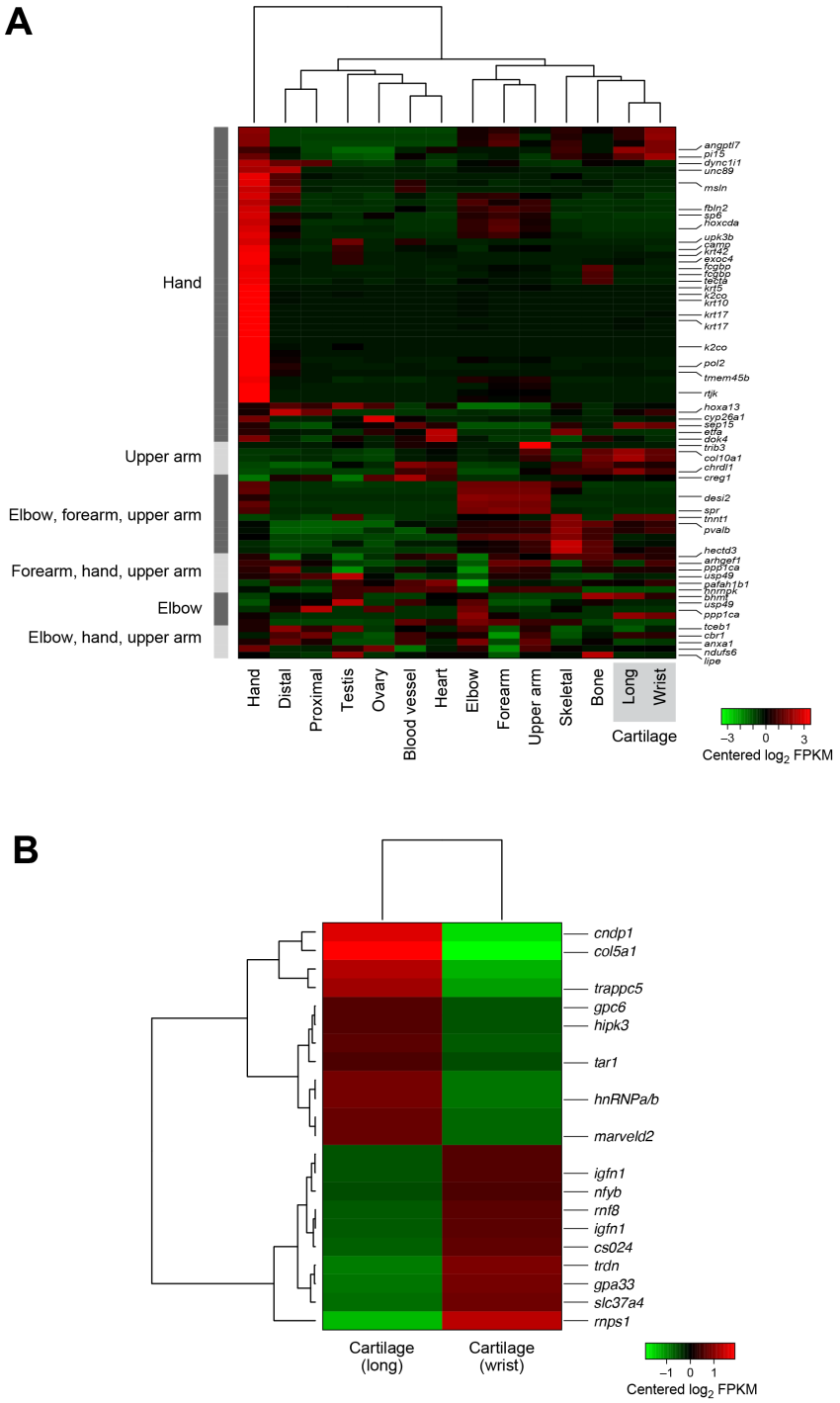

Figure S7. (A) Expression of arm-gradient enriched transcripts across all tissue types. Related to Figure 2 and Figure 6. Many arm segment enriched transcripts have transcriptional enrichment that largely reflects the tissue composition, such as relative skeletal muscle or cartilage content. Hand stands out as having a unique transcriptional program with many hand-specific transcripts being expressed. (B) A paucity of differentially expressed transcripts identified between wrist and long bone cartilage. Differences in expression between these two tissue types are subtle, and this bulk analysis of these two very similar tissue types likely simply lacks the resolution required to reveal key molecular differences between them.

Supplemental Tables

Table S1. Axolotl fastq read counts and Trinity assembly statistics. Related to Table 1 and Figure 1.
Attached as a separate file: Table_S1.fasq_read_counts_cegma_analysis.xls

Table S2. Tissue-enriched transcripts and Gene Ontology enrichment or depletion. Related to Figure 2.
Attached as a separate file: Table_S2.tissue_enriched_transcripts_gene_ontology.xls

Table S3. Differential isoform usage. Related to Figure 2.
Attached as a separate file: Table_S3.differential_isoform_usage.xls

Table S4. Blastema-enriched transcripts. Related to Figure 3.
Attached as a separate file: Table_S4.blastema_enriched_transcripts_listing.xlsx

Table S5. Arm-segment enrichment patterns, arm gradient correlations, and transcripts exhibiting enrichment in distal vs. proximal blastemas and vice versa. Related to Figure 6.
Attached as a separate file: Table_S5.proximal_distal_analysis.xls

File S1. Axolotl Trinity *de novo* assembly and Trinotate annotations. Related to Figures 1-6 and Table 1.

File S1A. Axolotl Trinity *de novo* assembly.
Attached as two separate files: File_S1A_Axolotl.TrinityAssembly.Part1.fasta.gz and File_S1A_Axolotl.TrinityAssembly.Part2.fasta.gz

File S1B. Trinotate annotations.
Attached as a separate file: File_S1B_Axo.Mar2014.Trinotate.xls.gz.

File S2. Transcript abundance, differential gene expression results, and gene ontology analyses. Related to Figures 1-3, Figure 5, and Figure 6.

File S2A. Differential expression results. In order to be included in this list, a transcript needed to be classified as differentially expressed by at least two differential expression algorithms.
Attached as a separate file: File_S2A_.Axolotl.TrinityAssembly.DiffExpressionMin2ProgsAgree.dat.gz. Zipped within File_S2_part_1.

File S2B. Gene ontology full results.
Attached as a separate file: File_S2B_.Axolotl.TrinityAssembly.GeneOntology.dat.gz. Zipped within File_S2_part_1.

File S2C. Raw transcript abundance counts produced with RSEM.
Attached as a separate file: File_S2C_.Axolotl.TrinityAssembly.RSEM_counts.matrix.gz. Zipped within File_S2_part_1.

File S2D. Normalized transcript abundance expressed as FPKM.
Attached as a separate file: File_S2D_.Axolotl.TrinityAssembly.TMM_normalized_FPKM.matrix.gz. Zipped within File_S2_part_1.

File S2E. Transcripts identified as differentially expressed by edgeR.
Attached as a separate file: File_S2E_.edgeR.trans.pairwise_summary.FDR0.05.dat.gz. Zipped within File_S2_part_2.

File S2F. Transcripts identified as differentially expressed by EBSeq.
Attached as a separate file: File_S2F_.EBSeq.pairwise.trans.post0.95.dat.gz. Zipped within File_S2_part_2.

File S2G. Transcripts identified as differentially expressed by MMDiff.

Attached as a separate file: File_S2G_.MMDIFF.trans.pairwise_summary.PostProb0.2.dat.gz. Zipped within File_S2_part_2.

Supplemental Experimental Procedures

Transcript abundance estimation and differential expression analysis

Counts of RNA-Seq fragments mapping to transcripts were determined for each tissue type using the RSEM software (Li and Dewey, 2011) (estimated RNA-Seq fragment counts per transcript are provided as **File S2C**, and TMM-normalized FPKM values provided as **File S2D**). The RSEM abundance estimates were input into edgeR (Robinson et al., 2010) and EBSeq (Leng et al., 2013) tools to identify differentially expressed transcripts in each of the pairwise tissue comparisons, employing a false discovery threshold of 0.05 (**Files S2E, S2F**). To further complement our DE analyses, we separately estimated expression values and identified differentially expressed transcripts using mmseq (Turro et al., 2011) and mmdiff (Turro et al., 2014), respectively. Transcripts defined by mmdiff as having a posterior probability of differential isoform usage >= 0.2 were captured as differentially expressed (**File S2G**). Transcripts found to be significantly differentially expressed by at least two of the DE analysis methods and to have at least a 2-fold change in expression were retained as candidate differentially expressed transcripts (**File S2A**) and subject to further analysis.

Computing the transcript contig E-statistic

Transcripts are ordered by expression values, and for each top-most *X* number of transcripts, the expression values are summed and the percentage of total expression represented by that set of transcripts is stated as the *E* percentage count of transcripts. For example, if the top *X* most highly expressed transcripts corresponds to 90% of the total expression data (by summing FPKM values), then E90 = *X*. The contig N50 statistic (Miller et al., 2010) is then computed for that corresponding set of transcripts. The contig N50 for the E90 set of transcripts is referred to as the E90N50 value. A script in the Trinity software suite is available for computing these transcriptome statistics and can be found as ${TRINITY_HOME}/util/misc/contig_ExN50_statistic.pl .

Identification of tissue-enriched transcripts

For each differentially expressed gene, a directed graph data structure was constructed with tissue types as nodes and directions of significant differential expression encoded by edges; an edge being drawn from up-regulated tissue *A* to down-regulated tissue *B* (for example, see **Figure 4A**). Those directed graphs that represented all tissue types were selected as best candidates for further study of tissue-enriched expression. Patterns of tissue-enriched expression were defined as collections of up- or down-regulated tissues, and genes were partitioned accordingly (**Table S3**). Genes exhibiting patterns of differential isoform usage were identified as those encoding at least two transcript isoforms, each significantly differentially expressed between at least two tissues, and demonstrating different patterns of tissue enrichment (**Table S5**). Tissue types for gill filament and embryo were excluded here due to not having biological replicates required for reliable detection of differentially expressed transcripts. The software we developed for identifying tissue-enriched transcripts is included in our Trinity software tool suite (https://github.com/trinityrnaseq/trinityrnaseq/tree/master/Analysis/DifferentialExpression/TissueEnrichment). Statistical enrichment of GO terms for groups of differentially expressed transcripts was performed using GO-Seq (Young et al., 2010).

Identification of transcripts expressed along a positional gradient in the limb

Transcript expression (TMM-normalized FPKM) values for arm segments were examined for significant Pearson correlation with ordered position as follows. Arm segments (upper arm, elbow, forearm, and hand) were assigned ordinal positions (1, 2, 3, 4). Those transcripts having at least a 2-fold difference in expression between the most distal positions (upper arm and hand) and having an expression of at least 1 TMM-normalized FPKM in any arm segment RNA-Seq replicate were tested for significant Pearson correlation with their ordinal positions using the *cor.test()* function in R (**Table S8**. Multiple testing corrections were performed via the Q-value method (Storey and Tibshirani, 2003)).

RNA Isolation and RT-PCR

Tissues were harvested while animals were deeply anesthetized (for limb specimens) or after they had been sacrificed (for all other specimens). RNA (from tissues described below) was isolated either by Trizol extraction or

by Qiagen RNeasy column for either library preparation or RT-PCR. For bone, ossified central areas of the humerus, radius, ulna, and metacarpals were isolated and immediately snap-frozen in liquid nitrogen. A similar approach was used for cartilage. Mortar and pestle were used to pulverize the tissue, which was immediately transferred to lysis buffer or Trizol. Soft tissues and embryos were placed directly in lysis buffer or Trizol. Blastemas were harvested at 23 days post-amputation (medium bud stage), and wound epidermis was manually removed prior to homogenization. DNase digestion (Qiagen RNase-free DNase) of genomic DNA, if required, was performed either on-column (for RNA purified by column) or following pellet resuspension (for RNA purified by Trizol). Following DNase treatment in suspension, samples were cleaned up by RNeasy MinElute column. RNA concentration was measured by spectrophotometer, and cDNA construction was performed using High Capacity cDNA Reverse Transcription Kit (Life Technologies) with template RNA seeded at 300 ng/20 µL reaction. Water was used in place of reverse transcriptase in the no-RT control reactions. Resulting cDNA was diluted 1:2 and used to seed RT-PCR reactions (1 µL in a 25 µL reaction). Standard NEB Taq was used for amplification, and RT-PCR reactions were conducted with 35 cycles. The entire reaction was loaded onto the gel. All RT-PCR results represent at least three individual biological replicates.

Morpholino design and delivery

Morpholinos were designed and synthesized by GeneTools. The *cirbp* targeting morpholino (5'-TTAGTTCTCTCGGATCAGGAGCACT-3') is predicted to bind upstream of the translational start site at -29 bp through -4 bp with respect to ATG. The standard control morpholino sequence is 5'-CCTCTTACCTCAGTTACAATTTATA-3'. The *kazald1* targeting morpholino (5'-TGGCAGCTCACAGTGACAGCCATTG-3') is predicted to bind 2 bp upstream through 23 bp coding sequence, while the control morpholino is the inverted sequence (5'-GTTACCGACAGTGACACTCGACGGT-3'). The sequence of the second *kazald1* targeting morpholino is 5'- ACAGTGCCACAAGTTTAGGTGACCA – 3', and the sequence for the corresponding alternative control morpholino is 5' – ACCAGTGGATTTGAACACCGTGACA – 3'. The second morpholino is predicted to bind upstream of the translational start site at -52 bp through -28 bp with respect to ATG. All morpholinos were conjugated to fluorescein at the 3' end to allow for electroporation and visualization. Morpholinos were reconstituted to 1 mM in 2x PBS and diluted to a working concentration of 500 µM in 1x PBS.

For *cirbp*, all four limbs of juvenile axolotls (6.0 – 8.0 cm. in length) were amputated proximally and electroporated with either PBS, standard control morpholino, or the *cirbp*-targeting morpholino. For *kazald1*, all four limbs of juvenile axolotls (5.0 – 8.0 cm. in length) were amputated proximally and electroporated with either *kazald1* targeting morpholinos or inverted control morpholinos at 10 days post-amputation (early to medium bud stage blastema). Each blastema was injected with ~0.5 - 1.0 µL of morpholino (500 µM), and all four limbs were used. For confirmation of Kazd1 and Cirbp protein knockdown, juvenile axolotls (5.0 – 6.5 cm. in length) were amputated proximally and electroporated at the early to medium bud stage (11 days post-electroporation). The vectors used for morpholino knockdown confirmation experiments (i.e. pCAG-tdTomato, pCAG-*kazald1*-myc, and pCAG-*cirbp*-myc) were diluted to a final concentration of 200 ng/µL prior to injection, and the morpholinos used were diluted to a final concentration of 500 µM. Our mock solution consisted of injection solution without vectors or morpholinos (i.e. 1x PBS with Fast Green dye to aid visualization). Following injection, electroporation was performed while animals were immersed in 1x PBS using a NepaGene Super Electroporator NEPA21 Type II electroporator. Our poring pulse consisted of 3 pulses at 150 Volts with a pulse length of 5 milliseconds, a pulse interval of 10 milliseconds, a decay rate of 0 %, and a positive (+) polarity. Our transfer pulse consisted of 5 pulses at 50 Volts with a pulse length of 50 milliseconds, a pulse interval of 950 milliseconds, a decay rate of 0 %, and a positive (+) polarity. The distance between electrodes for all electroporations was 3 millimeters.

Western Blotting

Protein samples were run on a 4 – 12% Bis-Tris gel and transferred to PVDF. Membranes were blocked in 5% milk (dissolved in 0.1% Tween 20 in Tris-buffered saline) and incubated with primary antibodies overnight at 4 °C. Following overnight incubation, secondary antibodies conjugated to horseradish peroxidase were added, and reactions were visualized using the ECL method (PerkinElmer: NEL103001EA). The primary antibodies used in this study were mouse anti-c-myc (1:500 dilution; Santa Cruz Biotechnology: sc-40) and rabbit anti-dsred (1:1000; Clontech: 632496). The secondary antibodies used were goat anti-rabbit HRP (1:5000; Jackson ImmunoResearch: 111-035-003) and goat anti-mouse HRP (1:5000; Bio-Rad: 1721019).

Cell Culture

Human embryonic kidney cells (HEK 293T) were used for experiments and maintained at 37°C in Dulbecco's Modified Eagle Medium (Life Technologies :11965-092) supplemented with 10% Fetal Bovine Serum. Cells were seeded approximately 24 hours prior to transfection. Immediately before transfection, cells were washed with PBS and placed into serum-free DMEM. Cells were then transfected with 1 μg of either pCAG-tdTomato, pCAG-*kazald1*-myc, or pCAG-*cirbp*-myc using polyethylenimine (PEI). Protein for western blotting was harvested at 24 hours post-transfection as described above.

Cloning and vector construction

The *kazald1* ORF was amplified from cDNA using primers 5'-CGAACAGAATTCCGCGCAATGGCTGTCACTGTGAGCTGCC -3' and 5' TGCCAAGCGGCCGCTTACAGATCTTCTTCAGAAATAAGTTTTTGTTCATCTCTATCCAGAGTTCCTTGCTC 3' (underscored letters bind *kazald1* ORF) and cloned into pCAG with EcoRI and NotI to create a version of pCAG-*kazald1*-myc that is targeted by *kazald1*-MO1. The *kazald1* ORF was amplified using primers 5' -CGAACAGAATTCTGGTCACCTAAACTTGTGGCACTGTCCCAGAATCCTTTGCTCTACACGCGCAATGGCTGTCACTGTGAGCTGCC -3' and 5' TGCCAAGCGGCCGCTTACAGATCTTCTTCAGAAATAAGTTTTTGTTCATCTCTATCCAGAGTTCCTTGCTC 3' (underscored letters bind *kazald1* ORF) and cloned into pCAG with EcoRI and NotI to create a version of pCAG-*kazald1*-myc that is targeted by *kazald1*-MO2. The *cirbp* ORF was amplified from cDNA using primers 5'-CGAACAGAATTCAGTGCTCCTGATCCGAGAGAACTAAGTCATGTCTTCGTCAGATGAAGG -3' and 5' TGCCAAGCGGCCGCTTACAGATCTTCTTCAGAAATAAGTTTTTGTTCGTTGTCATAATAGGATCCTC -3' (underscored letters bind *cirbp* ORF) and cloned into pCAG with EcoRI and NotI to create pCAG-*cirbp*-myc.

TUNEL assay

Tissue was harvested and fixed in 4% paraformaldehyde (PFA) in PBS for 1 hr, washed in PBS, and taken through a sucrose gradient to 30% sucrose in PBS. Specimens were embedded in OCT and frozen over dry ice/ethanol bath. Sections were cut at 16 μm on the cryostat, collected on Superfrost Plus slides (Fisher), and stored at -80^{o}C. Slides were later equilibrated to room temperature, rehydrated in PBS, and fixed in 4% PFA for 20 min, followed by 3 x 5 min washes in PBS. They were then incubated in cold permeabilization solution (PBS with 0.1% Triton X-100, 0.1% sodium citrate) at 4^{o}C for two min followed by immersion in 200 mL 0.1M sodium citrate pH 6.0 in the microwave for 1 min. Slides were cooled by adding 80 mL deionized water and then rinsed in PBS. They were blocked for 30 min at room temperature with 0.1M Tris-HCl (pH 7.5) and 3% BSA and 20% FBS. They were rinsed twice in PBS and then exposed to 100 μL of the TUNEL reaction enzyme mix (1:10) at 37oC for 1 hr. Slides were washed 3 x 5 min in PBS and mounted with Prolong Gold containing DAPI. Tissue sections were imaged at 4x on a Nikon Eclipse Ni microscope using NIS-Elements software. They were blindly scored by hand using ImageJ.

Alcian blue/alizarin red staining

Staining was performed as in (Whited et al., 2013).

CRISPR design, ribonucleoprotein complex preparation, and delivery

More details on the type II CRISPR-Cas9 system can be found in (Cong et al., 2013; Doudna and Charpentier, 2014). We designed our CRISPR RNA (crRNA) constructs by using the sgRNAcas9 software package to identify crRNAs, along with potential off-target sites, against the *kazald1* open reading frame based on our assembled transcriptome ((Xie et al., 2014)). The sgRNAcas9 software was run in "single" mode using default parameters. We identified two crRNAs that target the region spanning base pairs 73 to 95 of the *kazald1* open reading frame (region includes the PAM sequence). The sequence targeted by the first *kazald1* crRNA (crRNA-1)

including the PAM region (underlined) is: 5' CCCCGGCGTTTGCCCTTCAAGGG 3'. The sequence targeted by crRNA-1 is on the sense strand of the *kazald1* open reading frame. The sequence targeted by the second *kazald1* crRNA (crRNA-2) including the PAM region (underlined) is: 5' CCCTTGAAGGGCAAACGCCGGGG 3'. The sequence targeted by crRNA-2 is on the anti-sense strand of the *kazald1* open reading frame.

Recombinant Cas9 protein was purchased from PNA Bio Inc. (Catalog number: CP02) and reconstituted at a concentration of 5 µg/µL in UltraPure™ DNase/RNase-free distilled water (ThermoFisher Scientific; Catalog number: 10977023). The recombinant Cas9 protein had a 6 His tag and nuclear localization signal (NLS) from Simian virus 40 (SV40). Alt-R™ CRISPR Trans-activating RNA (tracrRNA), *kazald1* crRNA-1, and *kazald1* crRNA-2 were purchased from Integrated DNA Technologies and reconstituted at 100 µM in UltraPure™ DNase/RNase-free distilled water.

For injection of the CRISPR Cas9 ribonucleoprotein complex into embryos, tracrRNA and crRNAs were mixed at a 1:1 ratio and heated to 95 °C for 5 minutes. Following the 95 °C incubation, the tracrRNA:crRNA solution was kept on the thermocycler block and slowly cooled to room temperature. The two crRNAs used in this study were prepared separately, and control reactions consisted of tracrRNA mixed with an equal volume of UltraPure™ DNase/RNase-free distilled water. Once cooled, the tracrRNA:crRNA solution was mixed with recombinant Cas9 protein and incubated at 37 °C for 10 minutes and then cooled on ice to generate a working solution of the CRISPR Cas9 ribonucleoprotein complex. The working solution injected into embryos consisted of Cas9 at a final concentration of 500 ng/µL, tracrRNA at a concentration of 17.6 µM, and crRNA at a concentration of 17.6 µM. Wild type one-cell stage axolotl embryos (~90 % of injected embryos) and two-cell stage embryos (~10% of injected embryos) were collected and processed for injection as described previously (Khattak et al., 2009). Prior to injection, embryos across multiple wild-type batches were mixed together and randomly assigned to groups in order to minimize potential batch effects. Embryos at the one-cell stage were injected once with approximately 50 nanoLiters of working ribonucleoprotein complex solution or control solution (ribonucleoprotein complex without crRNA), while two-cell stage embryos received two 50 nanoLiter injections (one for each cell). Non-injected embryos were set aside as controls for batch viability. Injections were performed with a glass capillary needle.

More information on the electroporation of CRISPR-Cas9 RNPs into tissues and cell in culture can be found in (Chen et al., 2016; Kalebic et al., 2016; Liang et al., 2015; Shinmyo et al., 2016; Xu et al., 2016). For electroporation of the CRISPR Cas9 ribonucleoprotein complex into intact limbs, the ribonucleoprotein complex was assembled as described above. Following assembly, the ribonucleoprotein complex was mixed with the pCAG-EGFP plasmid, Fast Green dye (for visualization), and Dulbecco's Phosphate Buffered Saline solution (Life Technologies™; Catalog number: 14200-075). The working solution injected into intact axolotl forelimbs consisted of recombinant Cas9 at a final concentration of 1.67 µg/µL, tracrRNA at a concentration of 20 µM, crRNA at a concentration of 20 µM, pCAG-EGFP at a concentration of 209 ng/µL, and 1X Dulbecco's Phosphate Buffered Saline. The right forelimbs of juvenile axolotls (~ 6 – 7 cm. in length) were electroporated with 3 – 4 microliters of working ribonucleoprotein complex, and the left forelimbs of these axolotl were injected with 3 – 4 microliters of control solution (ribonucleoprotein complex without crRNA). Following injection, electroporation was performed while animals were immersed in 1x PBS using a NepaGene Super Electroporator NEPA21 Type II electroporator. Our poring pulse consisted of 3 pulses at 150 Volts with a pulse length of 5 milliseconds, a pulse interval of 10 milliseconds, a decay rate of 0 %, and a positive (+) polarity. Our transfer pulse consisted of 5 pulses at 50 Volts with a pulse length of 50 milliseconds, a pulse interval of 950 milliseconds, a decay rate of 0 %, and a positive (+) polarity. The distance between electrodes for all electroporations was 3 millimeters.

For studies that have pioneered the use of CRISPR-Cas9 and other genome editing technologies in the axolotl, please refer to (Fei et al., 2014; Flowers and Crews, 2015; Flowers et al., 2014; Kuo, 2015).

Genomic DNA extraction and T7 Endonuclease I digestion

We took tail clips from axolotl hatchlings (~ 3.5 weeks old) that were injected with the CRISRP Cas9 ribonucleoprotein complex or control hatchlings and extracted genomic DNA using the Qiagen DNeasy® Blood & Tissue Kit (Qiagen; Catalog number: 69506). We amputated intact limbs that were electroporated with the CRISPR Cas9 ribonucleoprotein complex at 25 days post-electroporation and isolated tissue that was EGFP positive using a

Leica M165 FC microscope to visualize fluorescence. We then extracted genomic DNA from the EGFP positive tissue using the Qiagen DNeasy® Blood & Tissue Kit.

We amplified genomic DNA samples using One *Taq*® DNA Polymerase (NEB; Catalog number: M0480L). PCR conditions were as follows: 94 °C for 3 minutes, then 35 cycles of 94 °C for 30 seconds, 57.2 °C for 30 seconds, and 68 °C for 15 seconds; the 35 cycles were followed by a 68 °C incubation for 5 minutes. The following primers were used to produce an amplicon of approximately 250 base pairs surrounding the region targeted by the *kazald1* crRNAs:
Primer 1: 5' CAGATCCTTGCCACTCTCCTGC 3'
Primer 2: 5' GCCATAGACTCGGTCAGACCTTGG 3'
PCR products were purified using Agencourt AMPure XP Beads (Beckman Coulter; Catalog number: A63881).

Following purification, 400 nanograms of amplified DNA were mixed with NEB Buffer 2 and re-annealed as follows: DNA was denatured at 95 °C for 5 minutes, cooled to 85 °C at -2 °C/second, and then cooled to 25 °C at -0.1 °C/second. Next, 20 units of T7 Endonuclease I (NEB; Catalog number: M0302L) was added to the reaction, and samples were incubated at 37 °C for 15 minutes. The digestion reaction was halted through the addition of EDTA to a final concentration of 17 mM and run on a 4% agarose gel. The expected size of the cleavage products produced from edited samples were approximately 200 base pairs and 50 base pairs for each crRNA. To calculate editing efficiency, ImageJ was used to quantify the band intensities of the wild-type product, cleavage products produced by T7 digestion, and background levels. Bands corresponding to apparent insertions or large deletions were also quantified. Following subtraction of background intensity from all measured band intensities for each lane, fractional cleavage was calculated as the sum of the cleaved product intensities divided by the sum of the intensities for all DNA bands for a given sample. Editing efficiency (Indel %) was calculated as:

$$\text{Indel } (\%) = 100\ x\ (1 - (1 - fraction\ cleaved)^{\frac{1}{2}})$$

Primers for *in situ* probes and RT-PCR
Genes and their associate primers are: *spatc1* (5' GCGTAAGATGGCCAGCGAAG 3', *5'* CAGAGGTCTTTTAATGATTTGTGATCTGG 3'), *tpm1* (5' GACCATTGACGATCTGGAAGATGAGC 3', 5' CCGACACAAAGCAAGAGGAATTGAG 3'), *ttn* (5' CAAGTGGATCAAATGGACTAAACTATC 3', 5' GCTTCCATGAGGGTAGTTGGAAAC 3'), *klhl41* (*5'* CATAAAGTGTGACTGCTGCTTCCAG 3', 5' CCTTTCATTGGGTCCTTTAATTACAACT 3'), *acta1* (*5'* CCAGAGCGCAAGTACTCTGTCT 3', *5'* CGGGTAGCATATTTAAGGTTTAT 3'), *col5a1* (*5'* CACTACCTCCCTCTACTGCCAC 3', *5'* CAGAGTGTGAGTGGAATGCTGC 3'), *ctsk* (*5'* GTGCAGAACCGACCCGATG 3', *5'* CAGCTGGACTCGGAGTGATGC 3'), *gspb1* (5' CCGCTTTGCTTCATCAACATATTGGGAG 3', 5' GGCAGGGCTGCTACTACAGCTAG 3'), *muc1* (*5'* GGGGGTTGAAGGTGTTGCTGATATTTC 3', 5' CTCATGATGCAACTGCAGAGCTTTCC 3'), *ef1a* (5' CGGGCACAGGGATTTCATC 3', 5' TGCCGGCTTCAAACTCTCC 3'), *cirbp* (5' CGACCCAGATGTCAAGATCCTCTTTAC 3', 5' CACCAGTCAAGCAAGTCACAAGCAAG 3'), *ptma* (5' GCTCTTGCGACTCGTCTTAGGCTTTG 3', 5' CAGGATGATCTTCAGACTCTTTCTCGGC 3'), *kazald1* (5' GAAAATGGATAAGGTGGTGGGGAGGG 3', 5' CTCGTGACATCCTGAGCCTGGAAG 3'), *sfrs1* (5' GCTATCCAGAGTAATGCAATTTTGTAGAGCC 3', 5' GACCATGACTAAAACAGTTTAACGGCACC 3'), *fus* (5' CCGATCTACCCAGCAAGCTGCC 3', 5' GTTGGCCATAACCACTCTGCTGCGC 3'), *hnrnpa1* (5' GGGCCCTGCAGAAGGTACGTTTATG 3', 5' GGGTTCTGGTTCAGTGCTACACAAGG 3'), *tecta* (5' GGCATAAGATGAAGAGGACTGATTGACAAC 3', 5' GAATTGGCAGTGCTGTTCAGTGCATATC 3'), *ef1a* (alternative, (Shaikh et al., 2011)) (5' AACATCGTGGTCATCGGCCAT 3', 5' GGAGGTGCCAGTGATCATGTT 3', *krt17* (5' GCCCAGTAACACCCTTGTCGGAG 3', 5' GGCGGTCGTTCAGGGTTTGCATG 3'), *shox2* (5' GCCATTGGCATTCACTCTCCAGGC 3', 5' CCCCATGACATAGAGGTGAAGGTCC 3'), and *cd38* (5' CAACAGGTAGATAGAGTATTTAACATTGTAGGC 3', 5' GGTGTGGTACATGTGATGCTGAATGG 3').

Supplemental References

Chen, S., Lee, B., Lee, A.Y., Modzelewski, A.J., and He, L. (2016). Highly Efficient Mouse Genome Editing by CRISPR Ribonucleoprotein Electroporation of Zygotes. J Biol Chem.

Cong, L., Ran, F.A., Cox, D., Lin, S., Barretto, R., Habib, N., Hsu, P.D., Wu, X., Jiang, W., Marraffini, L.A*., et al.* (2013). Multiplex genome engineering using CRISPR/Cas systems. Science *339*, 819-823.

Doudna, J.A., and Charpentier, E. (2014). Genome editing. The new frontier of genome engineering with CRISPR-Cas9. Science *346*, 1258096.

Fei, J.F., Schuez, M., Tazaki, A., Taniguchi, Y., Roensch, K., and Tanaka, E.M. (2014). CRISPR-mediated genomic deletion of Sox2 in the axolotl shows a requirement in spinal cord neural stem cell amplification during tail regeneration. Stem Cell Reports *3*, 444-459.

Flowers, G.P., and Crews, C.M. (2015). Generating and identifying axolotls with targeted mutations using Cas9 RNA-guided nuclease. Methods Mol Biol *1290*, 279-295.

Flowers, G.P., Timberlake, A.T., McLean, K.C., Monaghan, J.R., and Crews, C.M. (2014). Highly efficient targeted mutagenesis in axolotl using Cas9 RNA-guided nuclease. Development *141*, 2165-2171.

Kalebic, N., Taverna, E., Tavano, S., Wong, F.K., Suchold, D., Winkler, S., Huttner, W.B., and Sarov, M. (2016). CRISPR/Cas9-induced disruption of gene expression in mouse embryonic brain and single neural stem cells in vivo. EMBO Rep *17*, 338-348.

Khattak, S., Richter, T., and Tanaka, E.M. (2009). Generation of transgenic axolotls (Ambystoma mexicanum). Cold Spring Harb Protoc *2009*, pdb prot5264.

Kuo, T.-H., Kowalko, J. E., DiTommaso, T., Nyambi, M., Montoro, D. T., Essner, J. J., and Whited, J. L. (2015). TALEN-mediated gene editing of the thrombospondin-1 locus in axolotl. Regeneration *2*, 37-43.

Leng, N., Dawson, J.A., Thomson, J.A., Ruotti, V., Rissman, A.I., Smits, B.M., Haag, J.D., Gould, M.N., Stewart, R.M., and Kendziorski, C. (2013). EBSeq: an empirical Bayes hierarchical model for inference in RNA-seq experiments. Bioinformatics *29*, 1035-1043.

Li, B., and Dewey, C.N. (2011). RSEM: accurate transcript quantification from RNA-Seq data with or without a reference genome. BMC bioinformatics *12*, 323.

Liang, X., Potter, J., Kumar, S., Zou, Y., Quintanilla, R., Sridharan, M., Carte, J., Chen, W., Roark, N., Ranganathan, S*., et al.* (2015). Rapid and highly efficient mammalian cell engineering via Cas9 protein transfection. J Biotechnol *208*, 44-53.

Miller, J.R., Koren, S., and Sutton, G. (2010). Assembly algorithms for next-generation sequencing data. Genomics *95*, 315-327.
Robinson, M.D., McCarthy, D.J., and Smyth, G.K. (2010). edgeR: a Bioconductor package for differential expression analysis of digital gene expression data. Bioinformatics *26*, 139-140.
Shaikh, N., Gates, P.B., and Brockes, J.P. (2011). The Meis homeoprotein regulates the axolotl Prod 1 promoter during limb regeneration. Gene *484*, 69-74.
Shinmyo, Y., Tanaka, S., Tsunoda, S., Hosomichi, K., Tajima, A., and Kawasaki, H. (2016). CRISPR/Cas9-mediated gene knockout in the mouse brain using in utero electroporation. Sci Rep *6*, 20611.
Storey, J.D., and Tibshirani, R. (2003). Statistical significance for genomewide studies. Proc Natl Acad Sci U S A *100*, 9440-9445.
Turro, E., Astle, W.J., and Tavare, S. (2014). Flexible analysis of RNA-seq data using mixed effects models. Bioinformatics *30*, 180-188.
Turro, E., Su, S.Y., Goncalves, A., Coin, L.J., Richardson, S., and Lewin, A. (2011). Haplotype and isoform specific expression estimation using multi-mapping RNA-seq reads. Genome biology *12*, R13.
Whited, J.L., Tsai, S.L., Beier, K.T., White, J.N., Piekarski, N., Hanken, J., Cepko, C.L., and Tabin, C.J. (2013). Pseudotyped retroviruses for infecting axolotl in vivo and in vitro. Development *140*, 1137-1146.
Xie, S., Shen, B., Zhang, C., Huang, X., and Zhang, Y. (2014). sgRNAcas9: a software package for designing CRISPR sgRNA and evaluating potential off-target cleavage sites. PLoS One *9*, e100448.
Xu, L., Park, K.H., Zhao, L., Xu, J., El Refaey, M., Gao, Y., Zhu, H., Ma, J., and Han, R. (2016). CRISPR-mediated Genome Editing Restores Dystrophin Expression and Function in mdx Mice. Mol Ther *24*, 564-569.
Young, M.D., Wakefield, M.J., Smyth, G.K., and Oshlack, A. (2010). Gene ontology analysis for RNA-seq: accounting for selection bias. Genome Biol *11*, R14.